Longitudinal assessment of DREADD expression and efficacy in the monkey brain

Yuji Nagai[1,*], Yukiko Hori[1], Ken-ichi Inoue[2], Toshiyuki Hirabayashi[1], Koki Mimura[1], Kei Oyama[1], Naohisa Miyakawa[1], Yuki Hori[1], Haruhiko Iwaoki[1], Katsushi Kumata[3], Ming-Rong Zhang[3], Masahiko Takada[1], Makoto Higuchi[1], Takafumi Minamimoto[1,*]

[1]Advanced Neuroimaging Center, National Institutes for Quantum Science and Technology, Chiba 263-8555 Japan
[2]System Neuroscience Section, Center for the Evolutionary Origins of Human Behavior, Kyoto University, Inuyama 484-8506 Japan
[3]Department of Advanced Nuclear Medicine Sciences, National Institutes for Quantum Science and Technology, Chiba 263-8555 Japan

[*]Authors to whom all correspondence should be addressed:
Nagai Yuji, DVM, PhD
Takafumi Minamimoto, PhD
Advanced Neuroimaging Center
National Institutes for Quantum Science and Technology
4-9-1 Anagawa, Inage-ku, Chiba 263-8555 Japan
E-mails: nagai.yuji@qst.go.jp or minamimoto.takafumi@qst.go.jp

Abstract

Designer Receptors Exclusively Activated by Designer Drugs (DREADDs) offer a powerful means for reversible control of neuronal activity through systemic administration of inert actuators. Because chemogenetic control relies on DREADD expression levels, understanding and quantifying the temporal dynamics of their expression is crucial for planning long-term experiments in monkeys. In this study, we longitudinally quantified *in vivo* DREADD expression in macaque monkeys using positron emission tomography with the DREADD-selective tracer [^{11}C]deschloroclozapine (DCZ), complemented by functional studies. Twenty macaque monkeys were evaluated after being injected with adeno-associated virus vectors expressing the DREADDs hM4Di or hM3Dq, whose expression was quantified as changes in [^{11}C]DCZ binding potential from baseline levels. Expression levels of both hM4Di and hM3Dq peaked around 60 days post-injection, remained stable for about 1.5 years, and declined gradually after two years. Significant chemogenetic control of neural activity and behavior persisted for about two years. Virus titer and the presence of protein tags significantly influenced expression levels, with co-expressed protein tags reducing overall expression levels. These findings provide valuable insights and guidelines for optimizing the use of DREADDs in long-term primate studies and potential therapeutic applications.

Keywords

DREADDs, monkey, PET, AAV, nonhuman primates

Introduction

Chemogenetic technology affords remote and reversible control of neuronal activity by expressing receptors that are designed to be activated by systemically delivered biologically inert actuators. One such tool is the widely used Designer Receptors Exclusively Activated by Designer Drugs (DREADD) system, which is based on mutated muscarinic receptors (Roth, 2016). DREADDs have been widely used in rodent models and their use in nonhuman primates has recently shown some promise, as they could induce significant behavioral changes by simultaneously modulating activity of disparate neuronal populations across large brain regions (Eldridge et al., 2016; Nagai et al., 2016). Whether this promise will translate to reality depends on how long DREADDs can exert their effects. Because the efficacy of chemogenetic manipulation depends on DREADD expression levels (Grayson et al., 2016; Upright et al., 2018), maintaining high and stable expression levels is critical for ensuring consistent control throughout all experiments in a study. While this has proven possible in rodent studies that typically only span several months, whether it is true for studies involving macaque monkeys, which often last multiple years, remains a question. Indeed, despite the growing use of DREADDs in monkey neuroscience research, consistent and reliable data on the temporal dynamics of DREADD expression following viral transduction remain scarce. Specifically, little is known about how quickly DREADD expression is established following viral transduction or how long it is maintained. This gap in knowledge complicates efforts to optimize critical parameters, such as the serotypes, constructs, and titers of viral vectors that all influence expression level and duration.

Positron emission tomography (PET) is an *in vivo* imaging technique that allows quantification of receptor density in the brain. Several studies have demonstrated the utility of PET for longitudinal measurements of gene expression introduced into the brain via adeno-associated virus (AAV) (Nerella et al., 2023; Vandeputte et al., 2011; Yoon et al., 2014). While these studies have highlighted the potential of using PET imaging to monitor gene expression over time, most have used it as an indirect measure of target gene expression, without exploring the relationship between expression levels and the resultant functional outcomes.

Several PET probes have been developed to visualize DREADD receptor expression. Initial studies in rodents used [^{11}C]clozapine-N-oxide and [^{11}C]clozapine to monitor DREADD expression in the brain (Ji et al., 2016). In nonhuman primates, longitudinal PET studies using [^{11}C]clozapine have

successfully tracked virally expressed DREADDs in macaques (Nagai et al., 2016). More recently, DREADD-selective ligands such as [^{18}F]JHU37107 (Bonaventura et al., 2019) and [^{11}C]deschloroclozapine ([^{11}C]DCZ)(Nagai et al., 2020) have been developed. Among these, [^{11}C]DCZ has become a particularly useful tracer for studying DREADD-mediated functional manipulation in macaques and marmosets. This PET ligand allows researchers to verify the location and density of DREADD expression at the site of AAV injection and at projection sites, as demonstrated in numerous studies (Hirabayashi et al., 2024, 2021; Hori et al., 2021; Mimura et al., 2021; Miyakawa et al., 2023; Miyake et al., 2024; Mueller et al., 2023; Nagai et al., 2020, 2016; Oyama et al., 2024, 2022a, 2022b, 2021; Roseboom et al., 2021). Moreover, unlike post-mortem analysis that relies on the detection of fused or expressed protein tags, [^{11}C]DCZ PET provides a direct, quantitative, and non-invasive measure of DREADD expression level *in vivo*, using standard reference tissue models (Nagai et al., 2020; Yan et al., 2021). [^{11}C]DCZ PET thus serves as a valuable tool for tracking DREADD expression levels throughout long-term chemogenetics experiments in monkeys.

As the developer of the DREADD-selective agonist DCZ (Nagai et al., 2020), we have consistently performed multiple [^{11}C]DCZ PET scans as part of our DREADD experiments in monkeys, including at baseline before AAV injection, 30–120 days post-injection, and then periodically over the course of the experiments. For the current study, we analyzed these PET data to examine the short- and long-term dynamics of DREADD expression *in vivo* and assessed how these changes correlated with the ability to manipulate neuronal activity or behavior. Our results provide valuable information with a few caveats and indicate that the promise of using DREADDs in long-term monkey experiments is real.

Results

PET imaging data using [^{11}C]DCZ were collected from 15 monkeys before (baseline) and after injections of AAV vectors for expressing hM4Di or hM3Dq (see Table 1). To achieve neuron-specific expression, we used AAV vectors with a preference for neuronal infection, such as AAV2 or AAV2.1 (Kimura et al., 2023), or for incorporation with neuron-specific promoters (e.g., human synapsin promoter; hSyn). To assess the specific binding of [^{11}C]DCZ, we calculated the binding potential relative to a non-displaceable radioligand (BP_{ND}) using a multilinear reference tissue model with the cerebellum as a reference region (Yan et al., 2021). DREADD expression levels were then

quantified as the change in BP_{ND} (ΔBP_{ND}) from baseline values. This approach allowed us to longitudinally and quantitatively monitor the dynamics of DREADD expression *in vivo*.

Peak DREADD expression occurred approximately 60 days post-injection

To evaluate the temporal profile of DREADD expression and determine how quickly expression was established following transduction, we analyzed the [^{11}C]DCZ PET data from seven monkeys that received AAV vector injection into the subcortical regions of their brains (Tables 1 and 2). The data were selected according to the following criteria: (1) the titer of injected viral vector was 1.0–3.0×10^{13} gc/ml, (2) peak ΔBP_{ND} value was increased by more than 0.5, and (3) PET scans were repeatedly performed until 150 days post-injection. Analysis showed that expression levels of hM4Di and hM3Dq increased rapidly, reaching peak expression at approximately 60 days after viral vector injection. Notably, no clear differences in expression dynamics were observed between hM3Dq and hM4Di (Figure 1).

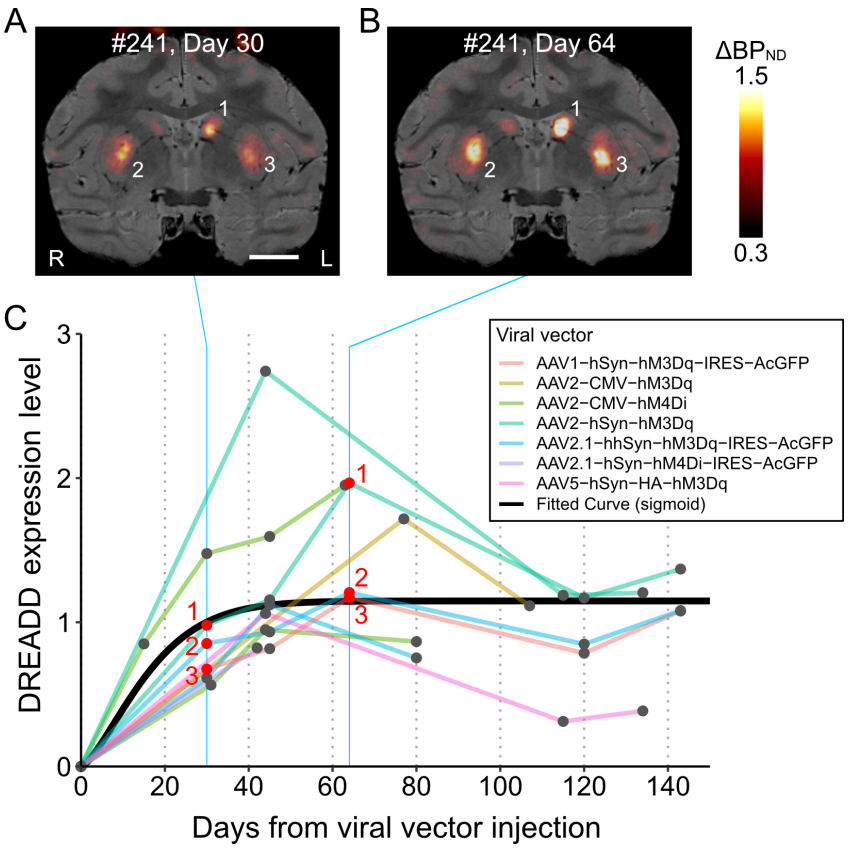

Figure 1 Time course of the DREADD expression levels up to 150 days after the injection

(**A, B**) Parametric coronal images of the increase (relative to baseline) in specific binding of [^{11}C]DCZ (ΔBP_{ND}) at 30 (A) and 64 (B) days after AAV injection, overlaid on MR images. Images were obtained from a monkey (#241) that received multiple injections of AAV with different constructs (see Table 2). (**C**) Time course of *in vivo* DREADD expression levels (ΔBP_{ND}) until 150 days after the injections, summarized from 10 ROIs obtained from 7 monkeys. The value at day 0 indicates the baseline (before injection). The red dots and numbers correspond to the value at the ROIs depicted in A and B. The black line is the best-fitted sigmoid curve.

Longitudinal assessment of DREADD expression levels

We then conducted a longitudinal assessment of post-peak expression levels for hM4Di and hM3Dq using repeated [^{11}C]DCZ PET measurements from 16 injection sites, including cortical and subcortical regions, across 11 monkeys. Figure 2 illustrates the temporal changes in normalized ΔBP_{ND}, expressed as a percentage of the peak value observed around 60 days post-AAV injection. hM4Di expression levels remained stable at peak levels for approximately 1.5 years before gradually declining after 2 years (Figure 2B). Compared with hM4Di, hM3Dq expression exhibited greater post-peak fluctuations, but nevertheless remained at ~75% of peak levels after about 1 year and declined to ~50% by 2 years post-injection (Figure 2C). This post-peak fluctuation was not explained by the cumulative number of times receptors were activated with DCZ (repeated measures two-way ANOVA, main effect of activation times, $F_{(1,6)}=5.745$, $p=0.054$).

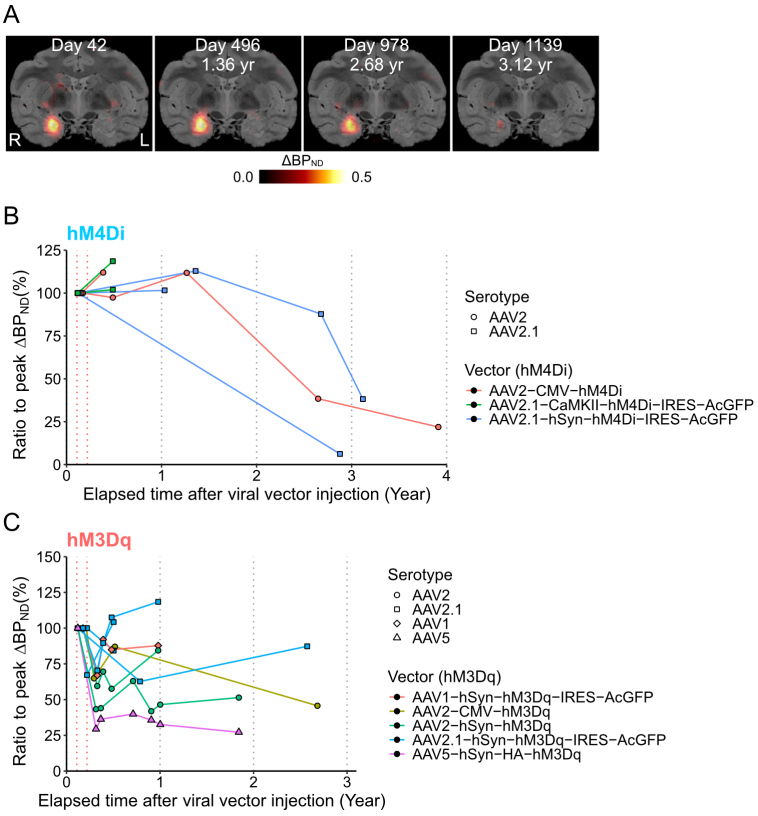

Figure 2 Longitudinal time-course of DREADD expression levels

(**A**) Parametric coronal images of DREADD expression levels (ΔBP_{ND}) overlaid on MR images obtained from monkey #237 measured at 42, 496, 978, and 1,139 days after injection. (**B-C**) Time course of hM4Di (**B**) and hM3Dq (**C**) expression as a ratio of peak expression level (ΔBP_{ND}). The dotted red vertical lines indicate the range of peak times across 11 monkeys (40 to 80 days). Expression levels of remained stable for about 1 (hM3Dq) or 1.5 years (hM4Di), after which they gradually decreased.

DREADDs effectively modulated neuronal activity and behavior for approximately two years

We assessed data from 17 monkeys to evaluate the duration over which DREADD activation produced significant effects on neural activity and behavior. Monkeys expressing hM4Di were assessed through behavioral testing (N = 11) and alterations in neuronal activity using electrophysiology (N = 2). Monkeys expressing hM3Dq were assessed for changes in glucose metabolism via [^{18}F]FDG-PET (N = 5) or alterations in neuronal activity using electrophysiology (N = 1). Across these assessments, significant chemogenetic effects were observed for up to three years following AAV vector injection (Figure 3). For example, one monkey with bilateral hM4Di

expression in the dorsolateral prefrontal cortex (dlPFC; monkey #229) consistently displayed impaired performance on the delayed response task with DCZ administration for up to 2.3 years (867 days) following vector injection (Oyama et al., 2021). Similarly, another monkey with hM3Dq expression in the amygdala (monkey #215) exhibited increased glucose metabolism following DCZ administration for up to 2.5 years (926 days) following vector injection, as measured by FDG-PET (Nagai et al., 2020).

Although experiment durations varied across monkeys, we consistently observed significant effects throughout the study periods, with only one monkey (#234) being removed from experiments due to a loss of DREADD effectiveness three years after transduction. In all other cases, receptor activation was performed repeatedly several tens of times, resulting in no clear loss of efficacy. After the termination of the chemogenetic studies, DREADD expression was verified by *in vitro* via postmortem immunohistochemical analysis (Fig. 3C-H). These findings highlight the robust and sustained functionality of DREADD systems in long-term experiments.

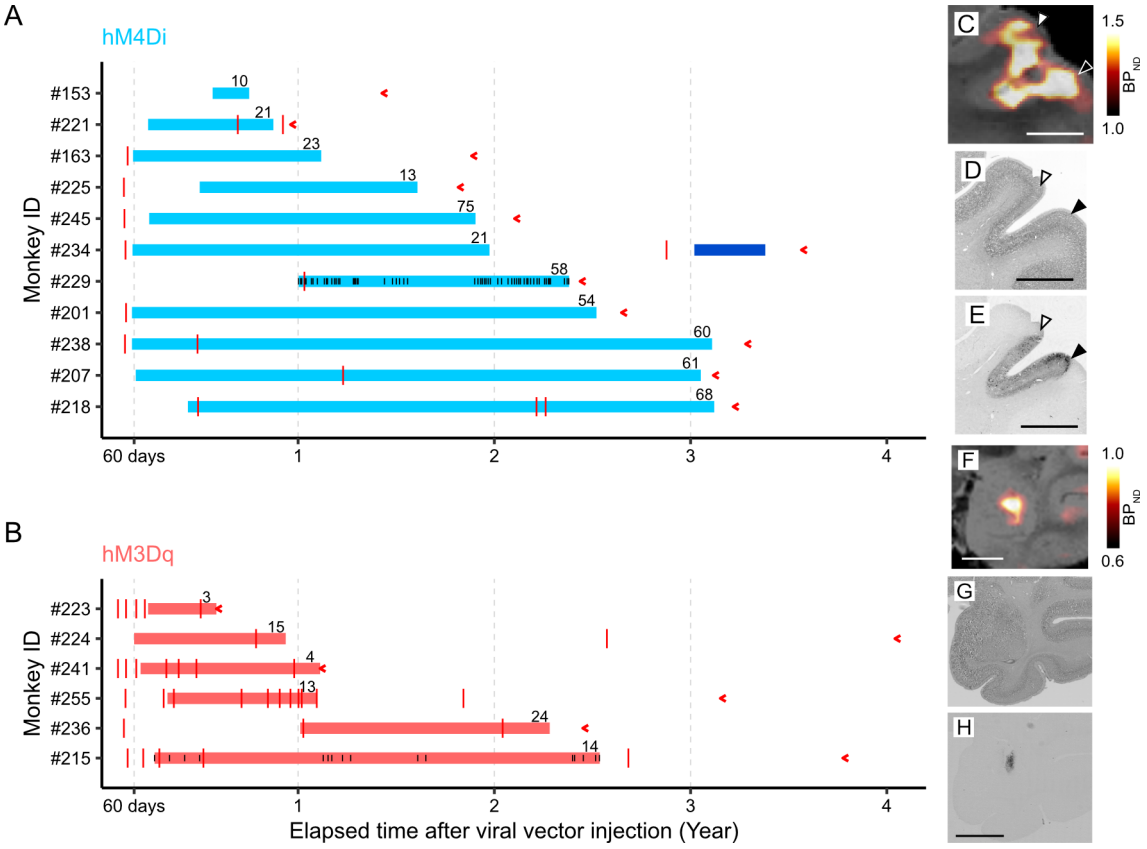

Figure 3 Duration of effective functional modulation induced by DREADDs

(**A-B**) Duration of effective functional modulation induced by hM4Di (**A**) and hM3Dq (**B**). Blue and

red horizontal bars indicate the duration of successful chemogenetic manipulation. For example, agonist administration (black tics) consistently induced behavioral change in monkey #229 and increased glucose metabolism in monkey #215. The corresponding functional assessments are summarized in Table 1. The dark blue bar indicates the duration of failed chemogenetic manipulation in monkey #234 (see Figure 4). Total numbers of agonist administrations (DREADD activation) are shown at the end of each duration bar. Red ticks indicate the timing of DCZ-PET scans, and red arrowheads indicate the timing of perfusion. (**C**) *In vivo* visualization of hM4Di expression in the dorsolateral prefrontal cortex 377 days after injection (monkey #229). The coronal PET image showing specific binding of [^{11}C]DCZ is overlaid on MR images. (**D and E**) Nissl- (**D**) and DAB-stained (**E**) sections corresponding to C, representing immunoreactivity against reporter protein. White and black arrowheads represent the dorsal and ventral borders of the target regions, respectively. Scale bars, 5 mm. (**F**) *In vivo* visualization of hM3Dq expression in the amygdala 980 days after the injection (monkey #215). The coronal PET image showing specific binding of [^{11}C]DCZ is overlaid on MR images. (**G and H**) Nissl- (**G**) and DAB-stained (**H**) sections corresponding to F, representing immunoreactivity against reporter protein.

As mentioned above, after more than three years, we observed the disappearance of hM4Di expression in one monkey (#234), and this was associated with the loss of chemogenetic behavioral effects. Specifically, activating hM4Di in the functionally defined representation of index finger primary somatosensory cortex (SI_{D2}) resulted in reversible behavioral deficits for two years, including impaired finger dexterity and hypersensitivity in the foot, confined to the contralateral side (Figure 4A)(Hirabayashi et al., 2021). However, *in vivo* imaging more than three years after injection indicated diminished hM4Di expression, and subsequent behavioral assessments failed to detect any motor deficits or hypersensitivity (Figure 4B). Post-mortem immunohistochemical examination confirmed the absence hM4Di, with no evidence of neuronal loss at the injection site (Figure 4C).

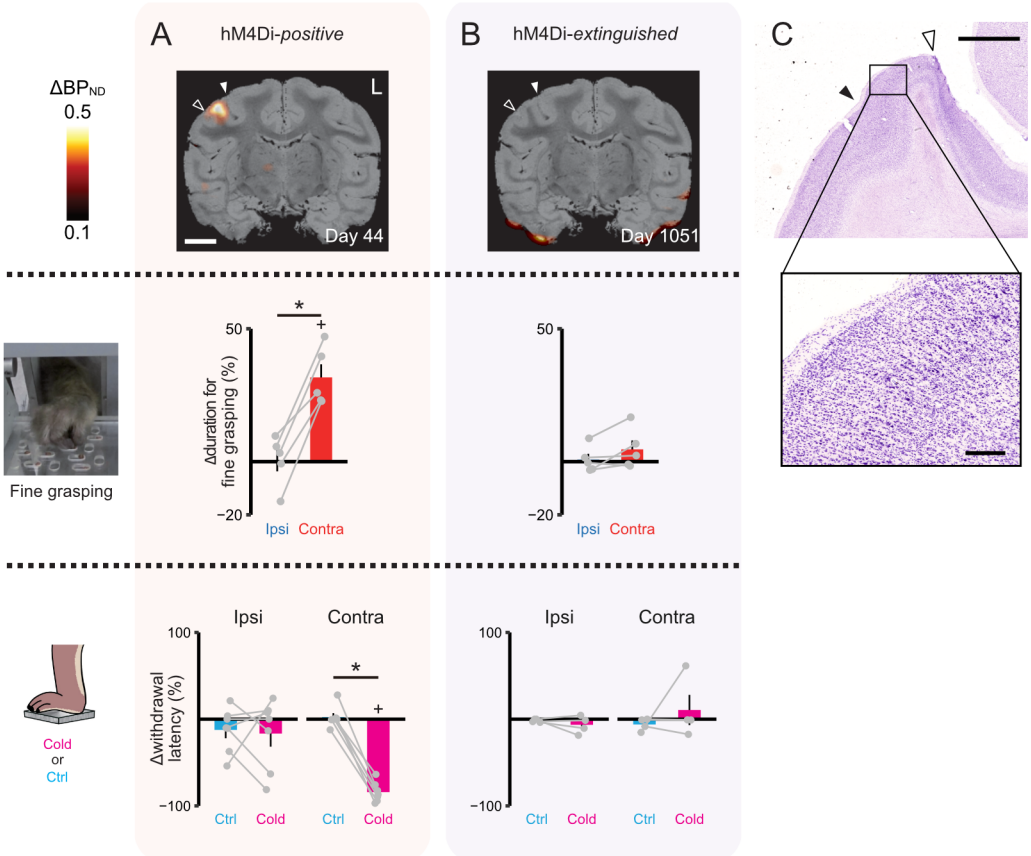

Figure 4 Disappearance of behavioral effects in an hM4Di-extinguished monkey (#234). (**A**) **Top**, Coronal PET image showing ΔBP_{ND} of [^{11}C]DCZ data overlaid on an MR image, obtained 44 days after viral vector injection into the right SI_{D2}. Filled and open arrowheads represent the central and ipsilateral sulci, respectively. **Middle**, Performance of fine grasping using a modified Brinkman board task, assessing the monkey's ability to pick up small food pellets with its thumb and index fingers. Values indicate the change in total duration to complete the task between pre- and post-DCZ administration sessions. *Ipsi* (*Contra*) refers to performance using the hand ipsilateral (contralateral) to the hM4Di-expressing SI_{D2}. Gray lines connect performances from the same sessions using different hands. Error bars, s.e.m. *: $P < 0.002$, paired t-test. +: $P < 0.004$, paired t-test, adjusted for multiple comparisons. n = 5 sessions. **Bottom**, DCZ-induced change in the withdrawal latency of the foot sole in response to cold (magenta) or control (cyan) stimulation. Negative values indicate faster withdrawal latency following DCZ administration. Gray lines connect performances from the same sessions. Error bars, s.e.m. *: $P < 0.001$, paired t-test. +: $P < 0.001$, paired t-test comparing between pre- and post-DCZ administration. n = 7 sessions. (**B**) Same measurements as in A, but following the extinction of hM4Di expression. The PET image was obtained about three years (1,051 days) post-vector injection. n = 5 and n = 4 sessions for Brinkman

board task and foot withdrawal test, respectively. (C) A Nissl stained section demonstrating the absence of neuronal loss at the vector injection sites. The locations of the filled and open arrowheads correspond to those shown in A and B. Scale bars are 2.5 mm and 250 μm.

Factors affecting DREADD expression levels

Finally, we investigated the factors influencing the level of DREADD expression. Despite examining expression across various cortical and subcortical brain regions, including the caudate nucleus, putamen, amygdala, thalamus, orbitofrontal cortex, dorsolateral prefrontal cortex, and SI, we found that peak expression level did not clearly depend on any specific brain area (one-way ANOVA, effect of brain region, $P = 0.154$). However, comparing peak expression among different viral vector constructs suggested several factors that might have influenced peak expression levels.

To identify these factors, we applied a linear model incorporating multiple variables, including serotype, promoter, titer, tag, and DREADD type. Our analysis revealed that virus titer, along with its interaction with DREADD type, significantly influenced expression levels (Table 3; Figure 5A). In addition, including co-expressed protein tags led to reduced peak expression levels, with the vector encoding the fusion HA-tag sequence at the 5'-terminal site (5'-HA) of the DREADD sequence exerting a stronger suppressive effect compared with the vector with GFP encoding following the internal ribosome entry site (IRES) sequence (Figure 5B).

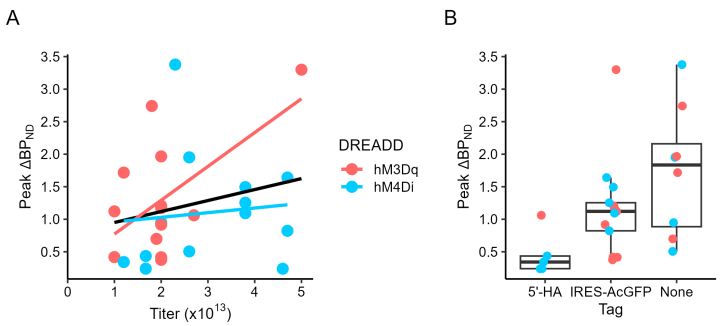

Figure 5 Peak DREADD expression levels among different viral vector constructs.
(**A**) Relationship between peak expression levels (ΔBP_{ND}) and virus titer. Regression lines are plotted for each DREADD (colored) and overall (black). (B) Peak expression levels (ΔBP_{ND}) for different constructs with the presence and type of protein tag. Box plots represent the median

(central line), interquartile range (box), and the range (whiskers) of the data. Points outside the whiskers indicate outliers.

Discussion

DREADDs have emerged as invaluable tools in nonhuman primate research due to their ability to exert effects on non-spatially restricted brain regions, allowing for simultaneous and discrete targeting of multiple areas. This capability makes DREADDs promising for investigating the causal roles of specific neural pathways and cell types in the highly specialized brain circuits found in primates. However, ethical and logistical constraints on using a large number of monkeys highlight the need of moving beyond a trial-and-error approach. It is essential to aggregate data and provide insights that are more widely applicable, thus enabling the development of a more efficient experimental design for DREADD research in monkeys. *In vivo* PET visualization of DREADDs offers a non-invasive and quantitative means for real-time monitoring of receptor expression. The present study analyzed PET and functional/behavioral data from 43 injection sites across 20 monkeys and revealed three key findings: (1) after AAV injection, DREADD expression levels peaked after approximately 60 days and remained stable for up to 1.5 years, followed by a gradual decline observed after two years; (2) significant chemogenetic effects on neural activity and behavior persisted for around two years; and (3) virus titer and protein tags significantly influenced peak expression levels, with co-expressed protein tags reducing peak expression. These results offer quantitative insights into the temporal dynamics of DREADD expression, thereby informing strategies for designing long-term experiments. They also confirm the efficacy and reliability of DREADD-mediated interventions.

Technical considerations

In vivo monitoring of gene expression has been conducted using fluorescent reporters observed through a window or fiber, providing a method to verify transducing protein expression and localization (Diester et al., 2011; Ruiz et al., 2013). Although useful for optogenetics or imaging studies, these methods are invasive, less quantitative, and spatially limited, often requiring cranial surgeries and capturing only two-dimensional data. In contrast, DCZ PET imaging provides a direct, non-invasive, volumetric measure of receptor expression, making it particularly suitable for studies in large animals such as macaques and for translational research with potential application to future human therapies.

Nevertheless, PET measurement has certain limitations, including potential variability due to individual differences, underestimation of DREADD expression levels due to the partial volume

effect, and the influence of anesthesia on kinetic parameters during imaging sessions. In this study, we have considered these factors and minimized their impact by applying appropriate ROI placements and excluding data collected under inadequate anesthetic conditions (see Methods).

Temporal dynamics of DREADD expression

Our [^{11}C]DCZ PET measurement showed that DREADD expression peaked around 60 days after AAV injection, regardless of whether hM4Di or hM3Dq was used. This pattern was consistent with our previous data of hM4Di expression visualized using [^{11}C]clozapine (Nagai et al., 2016). This gradual rise in AAV-mediated gene expression likely reflects rate-limiting steps following viral infection, including transport to the nucleus, uncoating, and conversion to double-strand DNA (Duan et al., 2000; Ferrari et al., 1996; Li and Samulski, 2020; Wang et al., 2007). Similar temporal patterns of AAV-mediated gene expression have been observed in previous studies using *in vivo* fluorescent measurement. For example, in rats transfected with an AAV5 encoding fluorescence protein (EYFP) in motor cortex and the hippocampus, *in vivo* fluorescence signals increased sigmoidally, rapidly until day 35, then slowed down (Diester et al., 2011). Similarly, in macaques, ChR2 expression monitored via fluorescence intensity peaked at around 60 days after AAV9 injection (Nakamichi et al., 2019).

Although our findings are based on a limited dataset targeting neuronal DREADD expression, they offer important insights for designing chemogenetics studies in primates. Specifically, beginning functional experiments at approximately 60 days post-AAV injection will yield reliable results, avoiding unnecessary delays. This timeline may also be applicable to other genetic studies in monkeys, such as those using optogenetics or calcium imaging, which also require proper expression of functional proteins. However, while these tools rely on rapid, light driven responses and are relatively less dependent on stable functional protein expression, DREADDs require sustained expression for consistent long-term effects.

Factors influencing DREADD expression

Our analysis indicated that both virus titer and the presence of protein tags significantly influenced DREADD expression levels. In general, while higher AAV titers result in increased transgene expression in neurons, excessively high titers can trigger immune responses, necessitating caution in their use. In the current study, we used titers that ranged from 1 to 5×10^{13} gc/ml, achieving a

balance between effective expression and minimal immune activation. Using vectors encoding DREADDs with protein tags, particularly 5'-terminal HA tags, was associated with a reduction of peak expression levels. Thus, although these tags are commonly used for antibody detection in DREADD constructs, they negatively impact expression efficacy and potentially affect protein function. Our findings are consistent with a previous PET study using [^{11}C]clozapine and immunohistochemical analysis, which also found reduced hM4Di expression in constructs with 5'-terminal HA tags (Nagai et al., 2016). Additionally, constructs incorporating IRES-GFP might also result in lower expression levels due to the size and composition of the AAV vector, as has been shown in previous studies (Furler et al., 2001; Kimura et al., 2023; Mizuguchi et al., 2000; Zhou et al., 1998). Nevertheless, these constructs have been frequently used in rodent research and have also been effective in producing long-term chemogenetic effects in monkey studies, including the current one (e.g., monkeys #229 and #238). Thus, while the observed decline in DREADD expression resulting from these constructs is not inherently detrimental to experimental outcomes in monkey studies, it serves as a warning that we must be careful when designing vectors to avoid reductions in experimental efficacy.

Implications for long-term experiments with DREADD expression

One of the most important findings was that AAV-mediated DREADD expression was maintained for up to 2 years for hM4Di and 1 year for hM3Dq. Throughout the duration of the experiments, chemogenetic effects remained consistent, as verified by individual behavioral and functional assessments. However, hM4Di expression diminished after 3 years, coinciding with the loss of chemogenetic behavioral effects in at least one case. This indicates that while chemogenetic effects can be maintained for up to two years, they likely decline gradually beyond this period. Consequently, researchers should anticipate consistent chemogenetic effects for a maximum of two years following AAV injection, and should be mindful that longer-term experiments risk a decline in effectiveness. Specifically, the inevitable failure to detect DREADDs via immunohistochemistry highlights an important caveat for researchers: timely termination of experiments to ensure verification through *in vitro* examination is necessary.

The gradual decline in expression levels observed beyond two years has several potential causes. First, AAV vectors typically remain episomal in transduced cells, without integrating into the host genome (Weitzman and Linden, 2011). While this poses less of an issue in non-dividing neurons,

episomal DNA can still be subject to gradual loss or degradation over time. Second, several mechanisms may contribute the gradual downregulation of transgene expression, including epigenetic modifications, immune responses, and genome stability (Muhuri et al., 2022). For example promoter silencing—often associated with epigenetic modifications—has been reported (Gray et al., 2011). Neuron-specific promoters have been shown to achieve more efficient and prolonged transgene expression than ubiquitous promoters like CMV (Paterna et al., 2000).

Our study found no evidence of cell death at AAV injection sites (Figure 4C), suggesting that neuronal loss was not a primary cause of the eventual decline in expression levels. Repeated receptor activation did not affect DREADD expression levels or chemogenetic efficacy in a previous study (Oyama et al., 2022). Thus, understanding the factors that contribute to the decline in expression remains of critical importance for developing optimal strategies to maintain persistent transgene expression in neurons, both for chemogenetic studies and therapeutic applications. Despite this uncertainty, our data offers important guidelines for chemogenetics studies in nonhuman primates, demonstrating that up to two years of reliable expression is achievable.

Translational implications

This research has significant translational implication, particularly for the development of DREADD-based therapies for treating neurological and psychiatric disorders. DREADD-based approaches have shown promising therapeutic potential, with successful application in monkey models of disease conditions such as epileptiform seizures (Miyakawa et al., 2023) and Parkinson's disease (Chen et al., 2023). Extending these findings to human clinical applications positions PET imaging as a powerful tool for real-time, non-invasive confirmation of target protein expression—a critical factor for ensuring therapeutic efficacy. PET reporter imaging has already shown its value in human gene therapy for certain movement disorders, where sustained protein expression has been correlated with treatment efficacy (Mittermeyer et al., 2012; Tai et al., 2022). Our study reinforces this utility by demonstrating that when DREADD expression was no longer detectable via PET, the chemogenetic effects were also diminished.

Conclusion

Our study describes short- and long-term dynamics of DREADD expression in nonhuman primates using [^{11}C]DCZ PET imaging, complemented by assessment of functional efficacy. The findings provide critical insights into the practicality of multi-year studies using chemogenetic

neuromodulation with DREADDs, including the expression time course and factors affecting expression stability. This work offers valuable guidance for designing future long-term nonhuman primate studies, and underscores the translational potential of using DREADDs combined with PET imaging for non-invasive, gene-targeted therapies for neurological and psychiatric disorders.

Methods

Subjects

A total of 20 macaque monkeys (10 Japanese, *Macaca fuscata*; 8 Rhesus, *Macaca mulatta*; 2 Cynomolgus, *Macaca fascicularis*; 16 males, 4 females; weight, 3.4–9.9 kg; age, 3–13 years at the beginning of experiments) were used (Table 1). The monkeys were kept in individual primate cages in an air-conditioned room. A standard diet, supplementary fruits/vegetables, and a tablet of vitamin C (200 mg) were provided daily. All experimental procedures involving animals were carried out in accordance with the Guide for the Care and Use of Nonhuman Primates in Neuroscience Research (The Japan Neuroscience Society; https://www.jnss.org/en/animal_primates) and were approved by the Animal Ethics Committee of the National Institutes for Quantum Science and Technology (11-1038).

Viral vector production

We used a total of 11 adeno-associated virus (AAV) vectors. AAV2-Syn-HA-hM3Dq, AAV2-Syn-HA-hM4Di, and AAV5-Syn-HA-hM4Di were purchased from Addgene (MA, USA). The other viral vectors were produced by a helper-free triple transfection procedure, which was purified by affinity chromatography (GE Healthcare, Chicago, USA). Viral titer was determined by quantitative polymerase chain reaction using Taq-Man technology (Life Technologies, Waltham, USA).

Surgical procedures and viral vector injections

Surgical procedures have been described in detail in the previous reports (Hirabayashi et al., 2021; Nagai et al., 2020, 2016; Oyama et al., 2023, 2022a, 2021). The AAV vectors and brain regions into which they were injected are summarized in Table 2. Before surgery, structural scans of the head were acquired via magnetic resonance (MR) imaging (7 tesla 400 mm/SS system, Bruker, Billerica, MA, USA) and X-ray computed tomography (CT) (Accuitomo170, J. MORITA CO., Kyoto, Japan) under anesthesia (continuous intravenous infusion of propofol 0.2–0.6 mg/kg/min). Overlay MR and CT images were created using PMOD® image analysis software (PMOD 4.4, PMOD Technologies Ltd, Zurich, Switzerland) to estimate the stereotaxic coordinates of target brain structures.

Surgeries were performed under aseptic conditions in a fully equipped operating suite. We monitored body temperature, heart rate, peripheral oxygen saturation (SpO_2), and endo-tidal CO_2 throughout all

surgical procedures. Monkeys were immobilized by intramuscular (i.m.) injection of ketamine (5–10 mg/kg) and xylazine (0.2–0.5 mg/kg) after i.m. injection of atropine sulfate (0.02–0.05 mg/kg) and then intubated with an endotracheal tube. Anesthesia was maintained with isoflurane (1%–3%, to effect). After surgery, prophylactic antibiotics and analgesics (cefmetazole, 25–50 mg/kg/day; ketoprofen, 1–2 mg/kg/day) were administered for 7 days.

Viral vectors were injected with a stereotaxic apparatus or a hand-held syringe. For stereotaxic injection, burr holes (~8 mm in diameter) were created for inserting the injection needle. Viruses were pressure-injected using a 10-µl Hamilton syringe (model 1701 RN, Hamilton, Reno, UV) mounted on a motorized microinjector (UMP3T-2, WPI, Sarasota, FL) held by a manipulator (model 1460, David Kopf, Tujunga, CA) on the stereotaxic frame. After making an approximately 3 mm cut in the dura mater, the injection needle was inserted into the brain and slowly moved down 1 to 2 mm beyond the target and then kept stationary for 5 min, after which it was pulled back up to the target location. Injection speed was 0.1 to 0.5 µl/min. After each injection, the needle remained *in situ* for 15 min to minimize backflow along the needle and then was pulled out very slowly.

For handheld injection, the target cortex of was exposed by removing a bone flap and reflecting the dura mater. Injections were made under visual guidance through an operating microscope (Leica M220, Leica Microsystems GmbH, Wetzlar, Germany) at an oblique angle to the brain surface. Each hemisphere received nine tracks of injections: one at the caudal tip, four along the dorsal bank, and four along the ventral bank of the principal sulcus, with 3 to 5 µL per track, depending on the depth (Oyama et al., 2023).

PET imaging

PET imaging was conducted as previously reported (Nagai et al., 2020). Briefly, PET scans were performed using a microPET Focus 220 scanner (Siemens Medical Solutions USA, Malvern, USA). Monkeys were initially immobilized with ketamine (5–10 mg/kg) and xylazine (0.2–0.5 mg/kg) and maintained under anesthesia with isoflurane (1%–3%) throughout the PET procedures. The isoflurane level was carefully adjusted to ensure the stability of continuously monitoring physiological parameters, such as body temperature, heart rate, SpO_2, and endo-tidal CO_2. Endo-tidal CO_2 levels were maintained between 35 and 45 mmHg to prevent substantial changes in cerebral blood flow (Markwalder et al., 1984), which could impact tracer kinetics. Transmission

scans were performed for about 20 min with a Ge-68 source. Emission scans were acquired in 3D list mode with an energy window of 350–750 keV after intravenous bolus injection of [^{11}C]DCZ (~350 MBq) and [^{18}F]FDG (~200 MBq). Data acquisition lasted for 90 min.

To estimate the specific binding of [^{11}C]DCZ, regional binding potential relative to a non-displaceable radioligand (BP_{ND}) was calculated by PMOD® with an original multilinear reference tissue model (MRTMo) (Yan et al., 2021). The cerebellum was used as a reference region, and t* was 15 min. The DREADD expression level was defined as ΔBP_{ND}, calculated by subtracting the pre-injection value from the post-injection value because the BP_{ND} value included off-target binding. This minimized individual differences because off-target binding varied among subjects. The volumes of interest (VOIs) reflecting DREADD expression were identified by drawing contours at half of the maximum ΔBP_{ND} value in the ΔBP_{ND} parametric image, which was smoothed with a 2 mm Gaussian filter, and overlaid onto the corresponding region in each individual MR image.

For the FDG study, DCZ (1 μg/kg) or vehicle was administered intravenously 1 min before FDG injection. Data were converted to Standardized Uptake Value (SUV) images, averaged between 30- and 60-min, and normalized to SUV ratio (SUVR) images using the mean whole-brain value. Metabolic changes induced by DCZ were calculated as ΔSUVR and defined by the different DCZ and vehicle conditions, with VOIs for FDG analysis matching those used in the [^{11}C]DCZ-PET study.

Administration of DREADD agonists

DCZ (HY-42110, MedChemExpress) and CNO (Toronto Research) were dissolved in dimethyl sulfoxide (DMSO FUJIFILM Wako Pure Chemical Co.), aliquoted, and stored at −30 °C. These stock solutions were then diluted in saline to a final volume of 0.1 ml (2.5% DMSO in saline), achieving a dose of 0.1 ml/kg and 3 mg/kg for DCZ and CNO, respectively. For behavioral testing, an agonist was injected 15 min before experiments began, unless otherwise noted. Fresh solutions were prepared on each day of usage.

Behavioral tasks

The behavioral experiments are summarized in Table 1. Complete descriptions of the detailed procedures for each behavioral experiment are available in the previous reports (Hirabayashi et al.,

2024, 2021; Hori et al., 2021; Oyama et al., 2024, 2022b, 2021). Here we focus on a modified Brinkman board task and a sensitivity to cold stimulation task, which were used to analyze the behavior of a monkey (#234) that had hM4Di expressed in its primary somatosensory cortex (Fig. 4). In the modified Brinkman board task, monkeys picked food pellets out of 10 slots in a board with one of their hands (i.e., contralateral or ipsilateral to the DREADD-expressing hemisphere), and the amount of time needed to pick up all ten items was recorded. The time to complete each trial was normalized to the number of pellets successfully picked up to obtain a value that reflected manual dexterity. In a single experimental session, the monkey performed five to ten trials with each hand before and 10 min after intravenous systemic administration of DCZ. In the sensitivity to cold task, monkeys were trained to place the sole of their foot on a cold metal plate that was placed in front of their monkey chair. The latency with which they withdrew their foot from the plate was recorded and used as an index of sensitivity to a cutaneous (cold) stimulus. If a monkey did not withdraw its foot within 60 s, the trial was terminated and a withdraw latency of 60 s was assigned for that trial. The monkeys performed five to ten trials for each of two temperature conditions (30°C for control and 10°C for cold stimulation) both before and 10 min after DCZ administration. Chemogenetic effects were assessed by comparing performance on the tasks pre- and post-injection and between contralateral and ipsilateral hands and feet (only the contralateral side should be affected by DCZ).

Statistics

All data and statistical analyses were performed using the R statistical computing environment (R Development Core Team, 2004). One way ANOVA was used to examine the relationship between vector injection sites (caudate, putamen, thalamus, amygdala, OFC, and SI) and peak expression level (peak ΔBP_{ND} value). Repeated measures two-way ANOVA was used to examine the effect of cumulative number of activation times × days after injection on post-peak fluctuation. A stepwise model selection using the MASS::stepAIC() function was performed to identify factors influencing the peak expression level. Starting with a full model that included five factors—virus titer, serotype, promoter, DREADD type, and tag—along with all their interactions, the best-fitting linear model was determined based on Akaike information criterion (AIC). The resulting best model included four variables, excluding serotype, and three interactions (Titer:DREADD type, Titer:Promoter, and DREADD type:Promoter). The significance of their contributions to the peak expression level, as well as the effect sizes (generalized eta squared), were assessed using Type II analysis of variance with the rstatix::anova_test() function.

Histology and immunostaining

For histological inspection, monkeys were deeply anesthetized with sodium pentobarbital (50 mg/kg, i.v.) or sodium thiopental (50 mg/kg, i.v.) after administration of ketamine hydrochloride (5−10 mg/kg, i.m.) and then transcardially perfused with saline at 4°C, followed by 4% paraformaldehyde in 0.1 M phosphate buffered saline (PBS, pH 7.4) at 4°C. The brain was removed from the skull, postfixed in the same fresh fixative overnight, saturated with 30% sucrose in phosphate buffer (PB) at 4°C, and then cut serially into 50-μm-thick sections on a freezing microtome. For visualizing immunoreactive GFP (co-expressed with hM4Di) signals, a series of every 6th section was immersed in 1% skim milk for 1 h at room temperature and incubated overnight at 4°C with rabbit anti-GFP monoclonal antibody (1:500, G10362, Thermo Fisher Scientific, Waltham, MA, USA) in PBS containing 0.1% Triton X-100 and 1% normal goat serum for 2 days at 4°C. The sections were then incubated in the same fresh medium containing biotinylated goat anti-rabbit IgG antibody (1:1,000; Jackson ImmunoResearch, West Grove, PA, USA) for 2 h at room temperature, followed by avidin-biotin-peroxidase complex (ABC Elite, Vector Laboratories, Burlingame, CA, USA) for 2 h at room temperature. For visualizing the antigen, the sections were reacted in 0.05 M Tris-HCl buffer (pH 7.6) containing 0.04% diaminobenzidine (DAB), 0.04% $NiCl_2$, and 0.003% H_2O_2. The sections were mounted on gelatin-coated glass slides, air-dried, and cover-slipped. Parts of other sections were Nissl-stained with 1% Cresyl violet. Images of sections were digitally captured using an optical microscope equipped with a high-grade charge-coupled device (CCD) camera (Biorevo, Keyence, Osaka, Japan).

Acknowledgements

This study was supported by MEXT/JSPS KAKENHI Grant Numbers JP19K08138, JP23K27098 (to YN), 24H00734 (to TH), 22H05157 (to KI), and JP20H05955 (to TM), by JST PRESTO Grant Numbers JPMJPR22S3 (to KO), by AMED Grant Numbers JP23wm0625001 (to TM) and JP24wm0625307 (to TH), and by the Moonshot Research & Development Program (Millennia Program) from JST Grant Number JPMJMS2295 (to TM and KI). Japanese monkeys were provided by the Japan MEXT National Bio-Resource Project “Japanese Monkeys”. We thank Jun Kamei, Ryuji Yamaguchi, Yuichi Matsuda, Yoshio Sugii, Takashi Okauchi, Risa Suma, Tomomi Kokufuta, Rie Yoshida, and Akari Ueshiba for their technical assistance.

Author contributions

Conceptualization: YN and TM; Resources: KI and KK; Investigation: YN, Yukiko H, TH, KO, and NM; Visualization: YN, KM, and TH; Formal analysis: YN, KM, and TH; Writing—original draft: YN, TH, and TM; Writing—review & editing: All authors.

Declaration of interests

The authors declare no competing interests.

Tables and Figures

Table 1. Summary of subjects, DREADD used, and functional assessments used in this study

ID	Species	Sex	weight (kg)	age (y)	DREADD	[^{11}C]DCZ	Behavior	FDG	Electrophysiology
153	R	M	6.8	10	hM4Di		✓*1)		
163	R	M	6.1	13	hM4Di		✓*2)		
193	R	M	4.4	9	hM4Di	✓			
201	R	M	6.3	8	hM4Di		✓*3)		✓
207	R	M	6.8	6	hM4Di		✓*3)		✓
212	R	F	3.4	8	hM4Di	✓			
218	J	M	7.2	4	hM4Di		✓*4)		
221	J	M	6.4	4	hM4Di	✓	✓*1)		
225	J	F	6	7	hM4Di	✓	✓*5)		
229	R	M	4.6	4	hM4Di	✓	✓*6)		
234	J	M	5.8	5	hM4Di	✓	✓*5)		
237	J	M	6.9	5	hM4Di	✓			
238	J	M	6.2	4	hM4Di	✓	✓*4)		
245	J	F	5.9	6	hM4Di	✓	✓*6)		
215	R	F	3.4	8	hM3Dq	✓		✓	
223	C	M	4.2	4	hM3Dq	✓		✓	
224	J	M	9.9	9	hM3Dq	✓			✓
236	J	M	7.1	6	hM3Dq	✓		✓	
241	J	M	5.1	3	hM3Dq	✓		✓	
255	C	M	5.2	4	hM3Dq	✓		✓	

R, Rhesus; *J*, Japanese; *C*, Cynomolgus; *M*, male; *F*, female. Weight and age are the values recorded at the beginning of the experiments. Behavior: *1) multi-reward task, #153 and #221, Oyama et al., *J Neurosci* 2022; *2) delayed-reward task, #163 Hori et al., *eLife* 2021; *3) delayed matching-to-sample task, #201 and #207, Hirabayashi et al., *Nat Comm* 2024; *4) reversal learning task, #218 and #238, Oyama et al., *Nat Comm* 2024; *5) Brinkman board/Foot sensation, #225 and #234, Hirabayashi et al., *Neuron* 2021; *6) delayed response task, #229 and #245, Nagai et al., *Nat Neurosci* 2020.

Table 2. Summary of injection location, type of virus vectors, titer, and injected volume used in this study

ID	Region	Vector	Titer ($\times 10^{13}$ gc/ml)	Volume (µl)
153	R-OFC	AAV2-CMV-hM4Di	1.0	54
	L-rmCD	AAV2-CMV-hM4Di	2.0	3
163	L-dCDh	AAV2.1-hSyn-hM4Di-IRES2-AcGFP	4.7	6
	R-dCDh	AAV2.1-hSyn-hM4Di-IRES2-AcGFP	4.7	6
193	R-Amygdala	AAV2-CMV-hM4Di	2.0	6
201	PET targeted R-OFC	AAV2-CMV-hM4Di	2.2	2
	PET targeted L-OFC	AAV2-CMV-hM4Di	2.2	2
207	PET targeted R-OFC	AAV2-CMV-hM4Di	1.3	3
	PET targeted L-OFC	AAV2-CMV-hM4Di	1.3	3
212	R-Put	AAV2-CMV-hM4Di	2.6	6
215	L-Amygdala	AAV2-CMV-hM3Dq	1.2	6
218	R-OFC	AAV2-CMV-hM4Di	2.3	50
	L-OFC	AAV2-CMV-hM4Di	2.3	54
221	L-OFC	AAV2-CMV-hM4Di	2.0	50
	R-rmCD	AAV2-CMV-hM4Di	2.0	3
223	R-Cd	AAV2.1-hSyn-hM3Dq-IRES2-AcGFP	1.0	3
	R-Put	AAV2.1-hSyn-hM3Dq-IRES2-AcGFP	5.0	3
	L-Cd	AAV2-CMV-hM3Dq-IRES-AcGFP	1.0	3
	L-Put	AAV2-hSyn-hM3Dq-IRES2-AcGFP	1.0	3
224	R-Amygdala	AAV2.1-hSyn-hM3Dq-IRES-AcGFP	2.0	5
	L-Amygdala	AAV2.1-hSyn-hM3Dq-IRES-AcGFP	2.0	4
225	L-SI_{D2} activation site	AAV2-CMV-hM4Di	1.54	4
229	R-dlPFC	AAV2.1-hSyn-hM4D-IRES2-AcGFP	4.7	35
	L-dlPFC	AAV2.1-hSyn-hM4D-IRES2-AcGFP	4.7	37
234	R-SI_{D2} activation site	AAV2.1-hSyn-hM4D-IRES2-AcGFP	3.8	4
236	R-Amygdala	AAV2-CMV-hM3Dq	1.2	6
237	L-Amygdala	AAV2.1-hSyn-hM4Di-IRES2-AcGFP	2.0	4
238	R-OFC	AAV2.1-CaMKII-hM4Di-IRES-AcGFP	1.0	49
	L-OFC	AAV2.1-CaMKII-hM4Di-IRES-AcGFP	1.0	53

241	R-Cd	AAV2-hSyn-hM3Dq-IRES-AcGFP	2.0	3
	L-Cd	AAV2-hSyn-hM3Dq	2.0	3
	R-Put	AAV2.1-hSyn-hM3Dq-IRES2-AcGFP	2.0	3
	L-Put	AAV1-hSyn-hM3Dq-IRES2-AcGFP	2.0	3
245	R-dlPFC	AAV2.1-hSyn-hM4D-IRES2-AcGFP	4.7	44
	L-dlPFC	AAV2.1-hSyn-hM4D-IRES2-AcGFP	4.7	40
255	L-VPL	AAV5-hSyn-HA-hM3Dq	2.7	3
	R-VPL	AAV2-hSyn-hM3Dq	1.8	3
	L-Cd	AAV2-hSyn-hM4Di	1.2	3
	R-Cd	AAV2-hSyn-hM4Di	4.6	3
	L-Put	AAV5-hSyn-hM4Di	1.67	3
	R-Put	AAV2-hSyn-hM4Di	1.67	3

R, right; *L*, left; *OFC*, orbitofrontal cortex; *rmCD*, rostromedial caudate nucleus; *dCDh*, dorsal part of caudate nucleus head; *CD*, caudate nucleus; *Put*, putamen; $S1_{D2}$, hand index finger region of primary somatosensory cortex; *dlPFC*, dorsolateral prefrontal cortex; *VPL*, ventral posterolateral nucleus of thalamus.

Table 3. Result of the linear model analysis

Effect	DFn	DFd	F-value	p-value	effect size (ges)
Titer	1	18	8.353	0.010*	0.317
DREADD	1	18	2.848	0.109	0.137
Promoter	2	18	1.116	0.349	0.110
Tag	2	18	5.274	0.016*	0.369
Titer:DREADD	1	18	4.835	0.041*	0.212
Titer:Promoter	1	18	1.404	0.251	0.072
DREADD:Promoter	1	18	1.911	0.184	0.096

DFn, degrees of freedom numerator; *DFd*, degrees of freedom denominator. *, $p < 0.05$.

The ANOVA table describing the factors contributing to the level of expression. The optimal model, selected based on Akaike's Information Criterion, was the following:

$$\Delta BP_{ND} = \textit{viral titer} + \textit{DREADD type} + \textit{promoter} + \textit{reporter-tag} + \textit{viral titer:DREADD type} + \textit{viral titer:promoter} + \textit{DREADD type:promoter}$$

The results indicate that the viral titer, reporter-tag, and the interaction between viral titer and DREADD type significantly affected DREADD expression levels.

References

Bonaventura J, Eldridge MAG, Hu F, Gomez JL, Sanchez-Soto M, Abramyan AM, Lam S, Boehm MA, Ruiz C, Farrell MR, Moreno A, Galal Faress IM, Andersen N, Lin JY, Moaddel R, Morris PJ, Shi L, Sibley DR, Mahler SV, Nabavi S, Pomper MG, Bonci A, Horti AG, Richmond BJ, Michaelides M. 2019. High-potency ligands for DREADD imaging and activation in rodents and monkeys. *Nat Commun* **10**:4627.

Chen Y, Hong Z, Wang J, Liu K, Liu J, Lin J, Feng S, Zhang T, Shan L, Liu T, Guo P, Lin Y, Li T, Chen Q, Jiang X, Li A, Li X, Li Y, Wilde JJ, Bao J, Dai J, Lu Z. 2023. Circuit-specific gene therapy reverses core symptoms in a primate Parkinson's disease model. *Cell* **186**:5394-5410.e18.

Diester I, Kaufman MT, Mogri M, Pashaie R, Goo W, Yizhar O, Ramakrishnan C, Deisseroth K, Shenoy KV. 2011. An optogenetic toolbox designed for primates. *Nat Neurosci* **14**:387–397.

Duan D, Yue Y, Yan Z, Yang J, Engelhardt JF. 2000. Endosomal processing limits gene transfer to polarized airway epithelia by adeno-associated virus. *J Clin Invest* **105**:1573–1587.

Ferrari FK, Samulski T, Shenk T, Samulski RJ. 1996. Second-strand synthesis is a rate-limiting step for efficient transduction by recombinant adeno-associated virus vectors. *J Virol* **70**:3227–3234.

Furler S, Paterna JC, Weibel M, Büeler H. 2001. Recombinant AAV vectors containing the foot and mouth disease virus 2A sequence confer efficient bicistronic gene expression in cultured cells and rat substantia nigra neurons. *Gene Ther* **8**:864–873.

Gray SJ, Foti SB, Schwartz JW, Bachaboina L, Taylor-Blake B, Coleman J, Ehlers MD, Zylka MJ, McCown TJ, Samulski RJ. 2011. Optimizing promoters for recombinant adeno-associated virus-mediated gene expression in the peripheral and central nervous system using self-complementary vectors. *Hum Gene Ther* **22**:1143–1153.

Grayson DS, Bliss-Moreau E, Machado CJ, Bennett J, Shen K, Grant KA, Fair DA, Amaral DG. 2016. The rhesus monkey connectome predicts disrupted functional networks resulting from pharmacogenetic inactivation of the amygdala. *Neuron* **91**:453–466.

Hirabayashi T, Nagai Y, Hori Y, Inoue K-I, Aoki I, Takada M, Suhara T, Higuchi M, Minamimoto T. 2021. Chemogenetic sensory fMRI reveals behaviorally relevant bidirectional changes in primate somatosensory network. *Neuron* **109**:3312-3322.e5.

Hirabayashi T, Nagai Y, Hori Yuki, Hori Yukiko, Oyama K, Mimura K, Miyakawa N, Iwaoki H,

Inoue K-I, Suhara T, Takada M, Higuchi M, Minamimoto T. 2024. Multiscale chemogenetic dissection of fronto-temporal top-down regulation for object memory in primates. *Nat Commun* **15**:5369.

Hori Y, Mimura K, Nagai Y, Fujimoto A, Oyama K, Kikuchi E, Inoue K-I, Takada M, Suhara T, Richmond BJ, Minamimoto T. 2021. Single caudate neurons encode temporally discounted value for formulating motivation for action. *Elife* **10**. doi:10.7554/eLife.61248

Ji B, Kaneko H, Minamimoto T, Inoue H, Takeuchi H, Kumata K, Zhang M-R, Aoki I, Seki C, Ono M, Tokunaga M, Tsukamoto S, Tanabe K, Shin R-M, Minamihisamatsu T, Kito S, Richmond BJ, Suhara T, Higuchi M. 2016. Multimodal imaging for DREADD-expressing neurons in living brain and their application to implantation of iPSC-derived neural progenitors. *J Neurosci* **36**:11544–11558.

Kimura K, Nagai Y, Hatanaka G, Fang Y, Tanabe S, Zheng A, Fujiwara M, Nakano M, Hori Y, Takeuchi RF, Inagaki M, Minamimoto T, Fujita I, Inoue K-I, Takada M. 2023. A mosaic adeno-associated virus vector as a versatile tool that exhibits high levels of transgene expression and neuron specificity in primate brain. *Nat Commun* **14**:4762.

Li C, Samulski RJ. 2020. Engineering adeno-associated virus vectors for gene therapy. *Nat Rev Genet* **21**:255–272.

Markwalder TM, Grolimund P, Seiler RW, Roth F, Aaslid R. 1984. Dependency of blood flow velocity in the middle cerebral artery on end-tidal carbon dioxide partial pressure--a transcranial ultrasound Doppler study. *J Cereb Blood Flow Metab* **4**:368–372.

Mimura K, Nagai Y, Inoue K-I, Matsumoto J, Hori Y, Sato C, Kimura K, Okauchi T, Hirabayashi T, Nishijo H, Yahata N, Takada M, Suhara T, Higuchi M, Minamimoto T. 2021. Chemogenetic activation of nigrostriatal dopamine neurons in freely moving common marmosets. *iScience* **24**:103066.

Mittermeyer G, Christine CW, Rosenbluth KH, Baker SL, Starr P, Larson P, Kaplan PL, Forsayeth J, Aminoff MJ, Bankiewicz KS. 2012. Long-term evaluation of a phase 1 study of AADC gene therapy for Parkinson's disease. *Hum Gene Ther* **23**:377–381.

Miyakawa N, Nagai Y, Hori Y, Mimura K, Orihara A, Oyama K, Matsuo T, Inoue K-I, Suzuki T, Hirabayashi T, Suhara T, Takada M, Higuchi M, Kawasaki K, Minamimoto T. 2023. Chemogenetic attenuation of cortical seizures in nonhuman primates. *Nat Commun* **14**:971.

Miyake T, Tanaka K, Inoue Y, Nagai Y, Nishimura R, Seta T, Nakagawa S, Inoue K-I, Hasegawa E, Minamimoto T, Doi M. 2024. Size-reduced DREADD derivatives for AAV-assisted multimodal chemogenetic control of neuronal activity and behavior. *Cell Rep Methods*

4:100881.

Mizuguchi H, Xu Z, Ishii-Watabe A, Uchida E, Hayakawa T. 2000. IRES-dependent second gene expression is significantly lower than cap-dependent first gene expression in a bicistronic vector. *Mol Ther* **1**:376–382.

Mueller SAL, Oler JA, Roseboom PH, Aggarwal N, Kenwood MM, Riedel MK, Elam VR, Olsen ME, DiFilippo AH, Christian BT, Hu X, Galvan A, Boehm MA, Michaelides M, Kalin NH. 2023. DREADD-mediated amygdala activation is sufficient to induce anxiety-like responses in young nonhuman primates. *Curr Res Neurobiol* **5**:100111.

Muhuri M, Levy DI, Schulz M, McCarty D, Gao G. 2022. Durability of transgene expression after rAAV gene therapy. *Mol Ther* **30**:1364–1380.

Nagai Y, Kikuchi E, Lerchner W, Inoue K-I, Ji B, Eldridge MAG, Kaneko H, Kimura Y, Oh-Nishi A, Hori Y, Kato Y, Hirabayashi T, Fujimoto A, Kumata K, Zhang M-R, Aoki I, Suhara T, Higuchi M, Takada M, Richmond BJ, Minamimoto T. 2016. PET imaging-guided chemogenetic silencing reveals a critical role of primate rostromedial caudate in reward evaluation. *Nat Commun* **7**:13605.

Nagai Y, Miyakawa N, Takuwa H, Hori Y, Oyama K, Ji B, Takahashi M, Huang X-P, Slocum ST, DiBerto JF, Xiong Y, Urushihata T, Hirabayashi T, Fujimoto A, Mimura K, English JG, Liu J, Inoue K-I, Kumata K, Seki C, Ono M, Shimojo M, Zhang M-R, Tomita Y, Nakahara J, Suhara T, Takada M, Higuchi M, Jin J, Roth BL, Minamimoto T. 2020. Deschloroclozapine, a potent and selective chemogenetic actuator enables rapid neuronal and behavioral modulations in mice and monkeys. *Nat Neurosci* **23**:1157–1167.

Nakamichi Y, Okubo K, Sato T, Hashimoto M, Tanifuji M. 2019. Optical intrinsic signal imaging with optogenetics reveals functional cortico-cortical connectivity at the columnar level in living macaques. *Sci Rep* **9**:6466.

Nerella SG, Michaelides M, Minamimoto T, Innis RB, Pike VW, Eldridge MAG. 2023. PET reporter systems for the brain. *Trends Neurosci* **46**:941–952.

Oyama K, Hori Y, Nagai Y, Miyakawa N, Mimura K, Hirabayashi T, Inoue K-I, Suhara T, Takada M, Higuchi M, Minamimoto T. 2021. Chemogenetic dissection of the primate prefronto-subcortical pathways for working memory and decision-making. *Sci Adv* **7**:eabg4246.

Oyama K, Hori Y, Nagai Y, Miyakawa N, Mimura K, Hirabayashi T, Inoue K-I, Takada M, Higuchi M, Minamimoto T. 2022a. Chronic behavioral manipulation via orally delivered chemogenetic actuator in macaques. *J Neurosci* **42**:2552–2561.

Oyama K, Hori Yukiko, Mimura K, Nagai Y, Eldridge MAG, Saunders RC, Miyakawa N,

Hirabayashi T, Hori Yuki, Inoue K-I, Suhara T, Takada M, Higuchi M, Richmond BJ, Minamimoto T. 2022b. Chemogenetic disconnection between the orbitofrontal cortex and the rostromedial caudate nucleus disrupts motivational control of goal-directed action. *J Neurosci* **42**:6267–6275.

Oyama K, Majima K, Nagai Y, Hori Yukiko, Hirabayashi T, Eldridge MAG, Mimura K, Miyakawa N, Fujimoto A, Hori Yuki, Iwaoki H, Inoue K-I, Saunders RC, Takada M, Yahata N, Higuchi M, Richmond BJ, Minamimoto T. 2024. Distinct roles of monkey OFC-subcortical pathways in adaptive behavior. *Nat Commun* **15**:6487.

Oyama K, Nagai Y, Minamimoto T. 2023. Targeted Delivery of Chemogenetic Adeno-Associated Viral Vectors to Cortical Sulcus Regions in Macaque Monkeys by Handheld Injections. *Bio Protoc* **13**:e4897.

Paterna JC, Moccetti T, Mura A, Feldon J, Büeler H. 2000. Influence of promoter and WHV post-transcriptional regulatory element on AAV-mediated transgene expression in the rat brain. *Gene Ther* **7**:1304–1311.

Roseboom PH, Mueller SAL, Oler JA, Fox AS, Riedel MK, Elam VR, Olsen ME, Gomez JL, Boehm MA, DiFilippo AH, Christian BT, Michaelides M, Kalin NH. 2021. Evidence in primates supporting the use of chemogenetics for the treatment of human refractory neuropsychiatric disorders. *Mol Ther* **29**:3484–3497.

Roth BL. 2016. DREADDs for neuroscientists. *Neuron* **89**:683–694.

Ruiz O, Lustig BR, Nassi JJ, Cetin A, Reynolds JH, Albright TD, Callaway EM, Stoner GR, Roe AW. 2013. Optogenetics through windows on the brain in the nonhuman primate. *J Neurophysiol* **110**:1455–1467.

Tai C-H, Lee N-C, Chien Y-H, Byrne BJ, Muramatsu S-I, Tseng S-H, Hwu W-L. 2022. Long-term efficacy and safety of eladocagene exuparvovec in patients with AADC deficiency. *Mol Ther* **30**:509–518.

Upright NA, Brookshire SW, Schnebelen W, Damatac CG, Hof PR, Browning PGF, Croxson PL, Rudebeck PH, Baxter MG. 2018. Behavioral effect of chemogenetic inhibition is directly related to receptor transduction levels in rhesus monkeys. *J Neurosci* **38**:7969–7975.

Vandeputte C, Evens N, Toelen J, Deroose CM, Bosier B, Ibrahimi A, Van der Perren A, Gijsbers R, Janssen P, Lambert DM, Verbruggen A, Debyser Z, Bormans G, Baekelandt V, Van Laere K. 2011. A PET brain reporter gene system based on type 2 cannabinoid receptors. *J Nucl Med* **52**:1102–1109.

Wang J, Xie J, Lu H, Chen L, Hauck B, Samulski RJ, Xiao W. 2007. Existence of transient

functional double-stranded DNA intermediates during recombinant AAV transduction. *Proc Natl Acad Sci U S A* **104**:13104–13109.

Weitzman MD, Linden RM. 2011. Adeno-associated virus biology. *Methods Mol Biol* **807**:1–23.

Yan X, Telu S, Dick RM, Liow J-S, Zanotti-Fregonara P, Morse CL, Manly LS, Gladding RL, Shrestha S, Lerchner W, Nagai Y, Minamimoto T, Zoghbi SS, Innis RB, Pike VW, Richmond BJ, Eldridge MA. 2021. [11C]deschloroclozapine is an improved PET radioligand for quantifying a human muscarinic DREADD expressed in monkey brain. *J Cereb Blood Flow Metab* **41**:2571–2582.

Yoon SY, Gay-Antaki C, Ponde DE, Poptani H, Vite CH, Wolfe JH. 2014. Quantitative, noninvasive, in vivo longitudinal monitoring of gene expression in the brain by co-AAV transduction with a PET reporter gene. *Mol Ther Methods Clin Dev* **1**:14016.

Zhou Y, Aran J, Gottesman MM, Pastan I. 1998. Co-expression of human adenosine deaminase and multidrug resistance using a bicistronic retroviral vector. *Hum Gene Ther* **9**:287–293.